JOURNAL OF MATERIALS SCIENCE 21 (1986) 1547–1552

The charge state of titanium ions implanted into sapphire: an EXAFS investigation

A. J. BOURDILLON, S. J. BULL, P. J. BURNETT*, T. F. PAGE
Department of Metallurgy and Materials Science, University of Cambridge, Pembroke Street, Cambridge CB2 3QZ, UK

X-ray absorption near-edge structure (XANES) and extended X-ray absorption fine structure (EXAFS) have been used to study the charge states and atomic environments of Ti^+ ions implanted into a single crystal sapphire substrate. Fluorescence techniques have been shown capable of detecting signals from the implanted ions even though the implant density in the $\sim 100\,\mu m$ thick specimen used is ~ 0.02 at% (the implant profile all being within $0.2\,\mu m$ of the surface). By comparison with TiO_2, Ti_2O_3 and TiO standards, XANES data suggest that the implant species environment is disordered. Further, EXAFS Fourier transforms show that the first shell radius of the implant species is between that of the TiO and Ti_2O_3 standards. Again, this indicates considerable structural disorder. After annealing the implanted specimen in air at 1150° C for 2 h, a shift towards the shell radius of the TiO_2 structure is observed together with a similar change in the XANES appearances. Our conclusion is that the initial titanium ion implant into sapphire exists in both the Ti^{2+} and Ti^{3+} charge states and is located in a range of sites in the radiation-damaged material. Annealing produces a shift in charge state towards Ti^{4+}. Implications for the solid solution hardening effect of the implant in sapphire are discussed.

1. Introduction

This paper presents the results of using X-ray absorption techniques to study the atomic environment and charge state of titanium ions implanted into sapphire.

Ion implantation is being increasingly used as a means of modifying the physical, chemical and mechanical properties of the near-surface regions of solids (e.g. [1–4]). Ion energies are typically in the range 0 to 0.5 MeV leading to the ions coming to rest in an approximately Gaussian distribution profile within $\leqslant 0.5\,\mu m$ of the surface. At high doses considerable concentrations ($\sim 50\%$) of ions may be introduced into this thin near-surface region. Radiation damage to the substrate accompanies implantation with considerable charge disturbance and hard-sphere displacements occurring. In ceramic materials, where the rate of room temperature dynamic annealing is low, cumulative displacement damage may eventually result in amorphization of the substrate. Amorphization begins at the peak of the damage profile and, with increasing dose, forms a sub-surface (and eventually a surface) amorphous layer which is usually mechanically soft compared to the original substrate (e.g. [2, 3, 5]. Prior to amorphization, the surfaces of many ceramics (e.g. SiC, MgO, Al_2O_3) show a progressive hardening with increasing dose (e.g. [2–4). However, it is unclear whether this hardening is due to radiation-hardening, solid-solution hardening from the implanted species or some combination of these effects.

In ceramic materials, solid-solution hardening effects are known to be more complex than the corresponding effects in metals. Current models correlate the extent of hardening with both the charge state and the detailed environment of the solute species in the solvent (e.g. [6]). In order to explore the possible extent of solid-solution hardening arising from the implantation of titanium into sapphire, we have sought an experimental technique capable of providing sub-surface information (since considerable structural relaxation may occur at the surface) about the state of specific ions which, in specimens considerably thicker than the implant profile, are only present in, on average, small concentrations.

X-ray absorption spectroscopy methods appear eminently suitable since they are powerful techniques for obtaining chemical and structural information about particular atomic species which can be selected from amongst those in a compound system by the measurement of characteristic absorption. The spectrum in the vicinity of the absorption edge can be divided into two regions: the X-ray absorption near-edge structure (XANES), which can be used to distinguish qualitatively one structure from a limited number of model structures [7], and the extended X-ray absorption fine structure (EXAFS) which consists of weak oscillations of the absorption coefficient above the absorption edge due to the interference of excited electrons with that part of their waves back-scattered from surrounding atoms. The oscillations exhibit periodicities of $2kR_j$ where R_j are the radii of

* *Present address*: Department of Metallurgy & Science of Materials, University of Oxford, Parks Road, Oxford OX1 3PH, UK.

0022–2461/86 $03.00 + .12

shells of atoms surrounding the characteristically excited one, and k is the wavenumber of the excited electrons concerned. Experimentally, k can be scanned using an X-ray spectrometer. Taking into account the phase shifts suffered by the electrons within the emitting atom potential, δ_1, and at the backscattering atom η, the fine structure function, $\chi(k)$, may be written, following Lee and Pendry [8], as;

$$\chi(k) = N_j/R_j|f(k)|^2\cos(2kR_j + 2\delta_1 + \eta)e^{-\sigma^2k^2}e^{-\gamma R_j} \quad (1)$$

where N_j is the co-ordination of shell j; $f(k)$ is the backscattering structure factor and the exponential terms are the usual Debye–Waller factor and a term describing absorption of the emitted wave by its surroundings. Thus, either by fitting experimental data to Equation 1 or by concentrating on the oscillating cosine term* through Fourier transform techniques, the atomic shell radii surrounding a selected species may be determined. In this paper, Fourier transform methods have been adopted since they provide the simplest means of comparing the observed shell radii from the system under study with known standards [9].

Conventionally, EXAFS is obtained from spectral measurements of X-ray transmission from a suitably thin specimen. However, since $f(k)$ is rather small (~ 0.3), data of a high statistical accuracy are required and, in dilute systems, the background noise may be sufficient to obscure the fine structure, or even the absorption edge itself. This can be overcome by measuring not the transmission of X-rays, but the characteristic fluorescence emission, which (competing with Auger emission) occurs after absorption. In this study, fluorescence EXAFS was used to obtain the near edge structure and fine structure due to the implanted titanium in sapphire where the average concentration (in $\sim 100\,\mu$m thick specimens) was as low as 0.02 at %. The need to use large area ($\sim 25\,\text{mm}^2$) specimens precluded the preparation of even thinner samples (e.g. using ion-beam thinning) where the average solute concentration would have been much higher.

2. Experimental details

Device substrate quality sapphire (α-alumina) wafers of $\{0\,1\,\bar{1}\,2\}$ section (courtesy of GEC, Wembley) were supplied with one side pre-polished to a mirror finish. A section of wafer ($\sim 25\,\text{mm} \times 25\,\text{mm} \times 0.4\,\text{mm}$) was implanted using the Cockcroft–Walton implantation facility at AERE Harwell, with 300 keV Ti^+ to a dose of $2.3 \times 10^{17}\,\text{ions cm}^{-2}$. For these ions, the projected range was 0.143 μm with a range straggling of 0.041 μm. The dose rate was a few $\mu\text{A cm}^{-2}$ and this caused a rise in specimen temperature of $\sim 200°$ C. The dose was measured by post-implantation Rutherford backscattering using 2 MeV He^+ ions in the IBIS Van der Graaff generator at AERE Harwell (e.g. see [5]).

In order to reduce the background noise during the EXAFS studies, the reverse (unimplanted) side of the specimen was polished (using diamond laps and cloths) to a thickness of $\sim 100\,\mu$m.

The specimen was mounted in a fluorescence EXAFS apparatus attached to the synchrotron radiation source (SRS) at the SERC Daresbury Laboratory. The incident radiation was focused in the vertical plane before monochromation by a channel-cut silicon (1 1 1) crystal. This beam then passed through an ion chamber intensity monitor before striking the specimen which was oriented to an arbitrary angle to avoid low index Bragg reflections being superimposed upon the spectrum. A further postspecimen ionization chamber provided transmission data.

The fluorescence detector was placed a short distance (~ 0.3 m) away from, and in good view of, the specimen in a horizontal direction perpendicular to the horizontally plane-polarized incident beam. The detector was a scintillator/photomultiplier combination mounted behind a beryllium window. Pulse height analysis of the amplified signal was used. Several spectra were aquired over a period of 10 h with an electron storage ring current of about 200 mA at 1.8 or 2 GeV. After checking that calibration shifts of the crystal spectrometer were less than twenty seconds of arc, spectra were added and are shown in Fig. 1.

The rate of data aquisition was much faster from the high-purity standard specimens, finely ground TiO_2 and TiO and coarsely ground Ti_2O_3, from which fluorescence and conventional transmission EXAFS were recorded. The specimen was then annealed in air for 2 h at 1150° C and further spectra obtained. From previous work [3], this heat treatment is known to both reduce the level of radiation damage and produce a variety of precipitates.

3. Results

3.1. XANES

At the absorption edge from the implanted titanium, the "white line" (i.e. the strong peak) is single and broad with little subsidiary structure (see Fig. 1a). This peak lies at an energy between that of the white line doublets observed in the standards (e.g. TiO_2, Figs. 1d, e, and Ti_2O_3, Figs. 1f, g). Although all the standards show doublets on the white line, there is some characteristic variation in height and width between them, the TiO and Ti_2O_3 peaks being of different heights while the TiO_2 peaks are of different widths. The structure exhibited by these standards is the same whether measured by fluorescence or by (less noisy) transmission (see Fig. 1). The structure due to the implanted titanium thus cannot be identified with any single oxide standard, but suggests the presence of a range of sites and charge states as might be expected in the damaged disordered structure.

After annealing, there is a dramatic change in the XANES of the implanted specimen, the two equally large peaks suggesting a structure tending towards that of TiO_2.

Since it seems that XANES provides a useful means of characterizing the chemical state of titanium ions in various Ti–O compound systems, the XANES from a

*This equation is frequently written with a sine term but a cosine term is equivalent if δ and η are redefined.

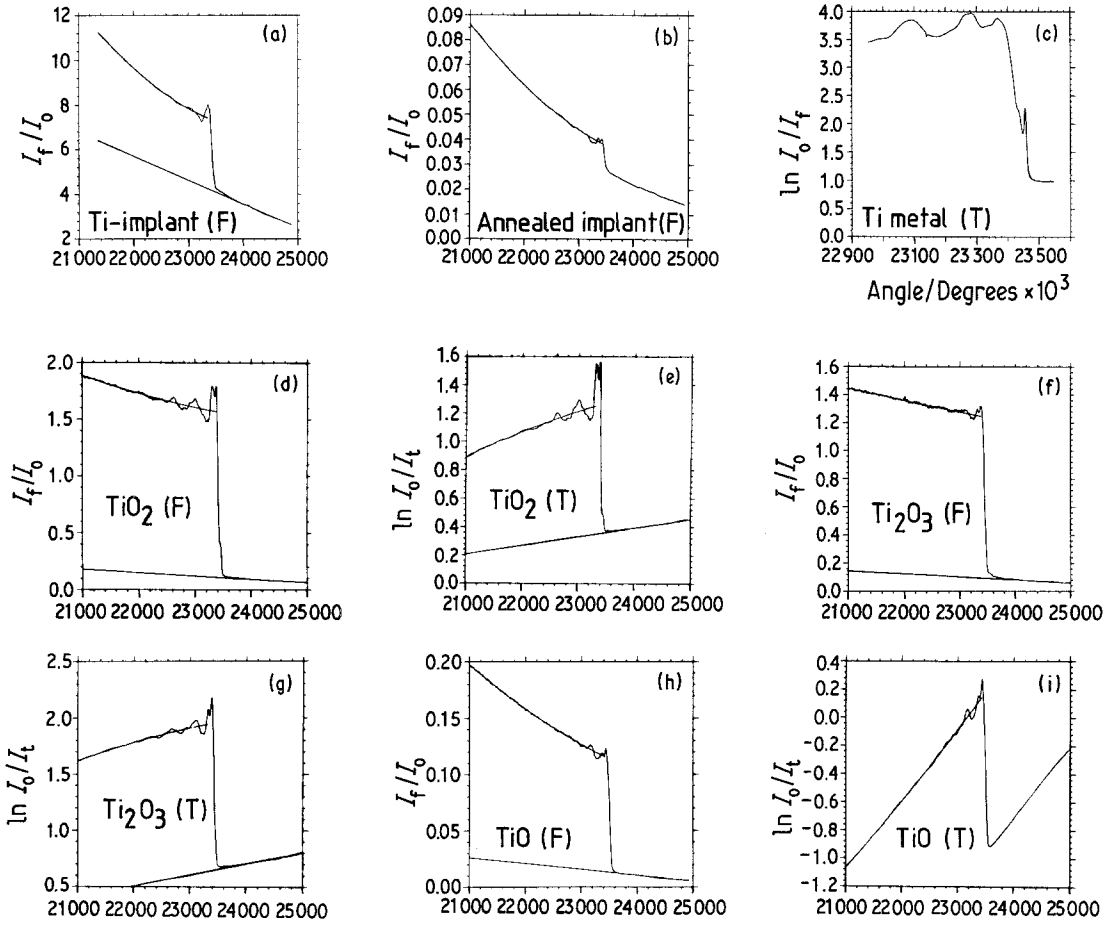

Figure 1 Flourescence (F) and transmission (T) spectra recorded in the vicinity of the titanium *K*-absorption edge in various samples. (a) Ti^+-implanted sapphire (F). (b) Ti^+-implanted sapphire after annealing at 1150° C for 2 h (F). (c) Titanium metal (T). (d) TiO_2 (F). (e) TiO_2 (T). (f) Ti_2O_3 (F). (g) Ti_2O_3 (T). (h) TiO (F). (i) TiO (T). In most cases, both the linear background fits (above the edge) and the pre-edge polynomial fits are shown.

pure titanium metallic system was measured to confirm that such distinct white lines did not occur. The spectrum is shown in Fig. 1c which shows no distinct white line. This can be understood if, in the oxides, the white line is due to bound s → p transitions (e.g. [10]) whereas in metallic titanium there is a continuum of excited states.

We shall now see if the chemical characterizations suggested by the XANES data are supported by EXAFS measurements of the first shell radius.

3.2. EXAFS

The jump ratios (i.e. edge height/background) of the fluorescence data for the implanted specimens (Fig. 1a and b) are naturally smaller than those for the standard specimens (Fig. 1d, f and g). After subtraction of the background by an extrapolated linear fit, μ_b, and after least squares polynomial fitting, $\mu_0(k)$, to the data $I(k)$ above the edge, the dimensionless fine structure was given by;

$$\chi(k) = \frac{I(k) - \mu_0(k)}{\mu_0(k) - \mu_b(k)} \qquad (2)$$

Here, for the fluorescence data, $I(k)$ was taken as the ratio of signal intensity/incident intensity, while for absorption data, it was taken as the carefully measured optical density, μx $(= \ln[I_0/I_t])$. Before Fourier transformation of the spectra, the abscissae angles were converted to corresponding energies and the point of zero energy (E_0) for the excited electron were consistently and accurately located at (arbitrarily) two thirds of the absorption edge height. Finally, E_0 was subtracted from the energy abscissae before conversion to momentum (k) space (Fig. 2).

By writing the phase shifts in equation 1 as a linear approximation, i.e. as $2\delta_1 + \eta \approx b - zak$, it will be seen that the real part of the Fourier transform;

$$r(R) = \int \chi(k) \exp(i2kR + b)\mathrm{d}k \qquad (3)$$

gives delta functions at $R = R_j - a$, broadened by the Debye–Waller factor etc., and by truncation, which also causes the imaginary part to be non-zero. This linear approximation is reasonably good for light elements [11] where scattering factors are comparatively well behaved. We now need to consider how this transform depends on the charge state and shell radius. *Prima facie*, the constants a and b might be expected to depend on charge state. However, the modulus of the transform (which is a type of radial distribution function) is found to be independent of b [12]. Further, a has been provisionally calculated [13] and at least partially experimentally demonstrated [14] to be largely independent of charge state. Thus, the modulus of the Fourier transform is approximately independent of a and b and so changes in peak positions observed in the Fourier transforms of the

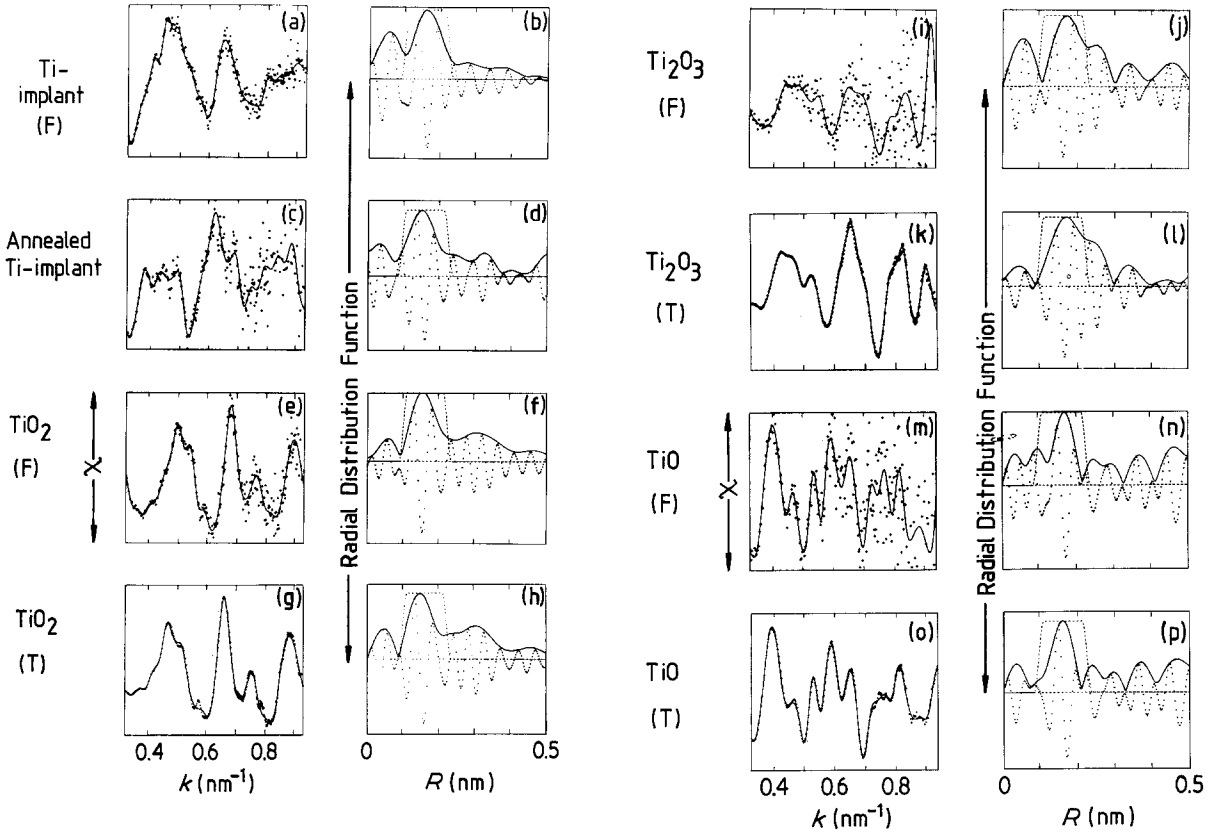

Figure 2 Weighted ($\times k^3$) EXAFS spectra (a, c, e, g, i, k, m, o) together with the moduli (lines) and real parts (dots) of the corresponding Fourier transforms (b, d, f, h, j, l, n, p) for the flourescence (F) and transmission (T) spectra shown in Fig. 1. The transmission spectra are intrinsically less noisy than the fluourescence spectra and the shifts in the Fourier transform peaks resulting from this noise give a measure of the experimental error (see text). The dashed window in (b, d, f, h, j, l, n, p) is located on the first shell radius.

measured EXAFS can be interpreted directly as changes in shell radii.

The data shown in Fig. 2 have been analysed using identical truncation limits. It is interesting to observe that the transforms of the more statistically reliable absorption data (Fig. 2) are very similar to those of corresponding fluorescence spectra (except for an apparently spurious spike at 22° in Fig. 1f, which does not affect the following analysis). In fact, the inferior statistics of the fluorescence spectra actually result in slight shifts of the peak in the modulus, when compared to the absorption data from the same specimen, and these shifts provide a measure of the errors in the peak positions (~ 0.004 nm). We can now interpret these data by comparing the implant first shell radius with atomic separations in various titanium oxides. Values of $(R - a)$ were calculated by taking the peak centres as bisecting the 0.75 peak height widths from the transforms of Figs. 2b, d, h and p and at 0.85 peak height width for Fig. 2l (where the first and second shells overlap).

Fig. 3 shows these $(R - a)$ values for the TiO, Ti_2O_3 and TiO_2 samples plotted against nominal charge state (i.e. 4+ for Ti in TiO_2 etc.). The values determined for the implanted and annealed sample are also shown. In order to calculate the value of a (and hence the shell radius R), it is necessary to make comparisons with the known bond lengths in the various standards. As described by Wyckoff [15], the various oxides of titanium contain a range of Ti–O separations, namely 0.2088 nm in TiO; 0.201 to 0.208 nm in Ti_2O_3; 0.195 to 0.198 nm in TiO_2 (rutile); 0.191 to 0.195 nm in TiO_2 (anatase) and 0.187 to 0.204 nm in TiO_2 (brookite). These values are also plotted against charge state on the right-hand side of Fig. 3. The parameter a can be calculated from the difference between the Wyckoff values of R and the EXAFS $(R-a)$ values. Good agreement is found for the cases of TiO ($a = 0.045$ nm) and the mean value for the three polymorphs of TiO_2 ($a = 0.046$ nm). The agreement for Ti_2O_3 is less good, presumably due to the overlapping shells noted above. If the Ti_2O_3 data are regarded as unreliable, then the near constant value of a for TiO and TiO_2 confirm the independence of a from charge state as assumed earlier in this section.

Using the above value of a, first shell radii were calculated for the implanted and annealed specimens and are shown as vertical lines on the right-hand side of Fig. 3. It can be seen that the R value for the implanted sample lies between the value for TiO and Ti_2O_3 while that for the implanted and annealed sample is shorter, lies between those for Ti_2O_3 and TiO_2 and has moved towards the TiO_2 polymorphs. Since there is no simple agreement between the first shell radius for the titanium implant and any standard, it would seem that there is some disorder in the structure around the titanium sites (and hence in the effective charge on the titanium ions). This is consistent with the XANES observations. However, after annealing, the development of higher shell structures (e.g. at 0.33 nm in Fig. 2d, c.f. Fig. 2b)

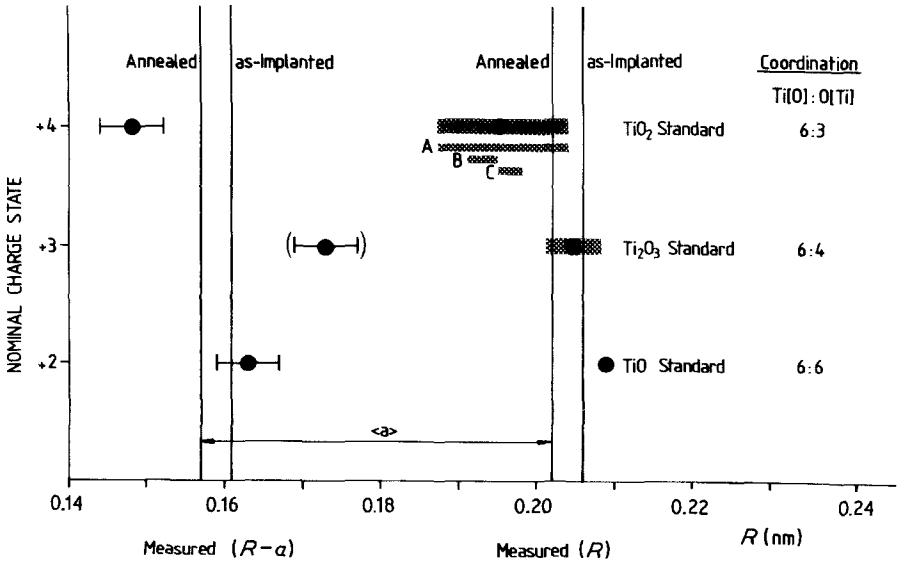

Figure 3 A graphical representation of the $(R - a)$ values as measured by EXAFS plotted as a function of nominal charge state (left-hand side) and coordination. $(R - a)$ values for the as-implanted and implanted-and-annealed samples are shown as vertical lines. The right-hand side of the diagram shows the reported first-shell radii for titanium ions in the TiO, Ti_2O_3 and TiO_2 standards [15]. The shaded regions show the Ti–O bond length ranges in Ti_2O_3 and the polymorphs of TiO_2 (brookite, A; anatase, B; and rutile, C. The value of a is seen to be virtually constant for the TiO and TiO_2 standards and less reliable for Ti_2O_3 (data point bracketted) because of overlapping second shells (see text). Using the TiO_2/TiO value of a, R values have been calculated for the as-implanted and implanted-and-annealed samples and are again shown as vertical lines. For the as-implanted sample, R is seen to lie between the values for TiO and Ti_2O_3, while annealing shortens R towards the TiO_2 value (see text).

indicates that some degree of ordering has resulted, as might be expected. Even so the calculated bond length (0.202 nm) for this case is considerably larger than that for Al–O in sapphire (0.191 nm) showing that titanium is not simply substituted into the α-Al_2O_3 structure.

Thus, the three types of evidence available from the data described here (i.e. XANES and first and higher EXAFS shell radii) all indicate that the implanted atoms occupy disordered sites of ill-defined charge state especially in the as-implanted state. The presence of structural disorder implies that radiation annealing during implantation is not sufficient to render the structure perfect even at a highly localized level. Subsequent thermal annealing improves that state of order.

4. Discussion and conclusions

The results presented in the previous section indicate that, prior to annealing, there is no one chemical state for titanium ions implanted into sapphire, an apparent mixture of Ti^{2+} and Ti^{3+} being observed. This is in qualitative agreement with the conversion electron Mössbauer studies made on $^{57}Fe^+$ implanted into MgO [16] where it was found that Fe^{2+} was the predominant species with some Fe^{3+} and metallic ion also being present. The proportion of the states present depended upon dose. In the present study, only one dose has been investigated. However, within this implanted layer the Gaussian nature of the damage and concentration profiles results in a range of structures and solute levels. Thus, a range of implant states and environments are also to be expected.

In addition, channelled-Rutherford backscattering studies [3] indicate that the implanted layer in our specimen in fact consists of a sub-surface amorphous layer surrounded by damaged but crystalline material. Thus, although something about the average charge state in the layer has been deduced, the depth distribution of these states and their spatial correlation with the structural disorder present, still remains uncertain.

Preliminary XPS studies on a wedge shaped specimen that allowed the whole of the implanted layer to be sampled [17] also suggested that sapphire implanted to a dose of 2.3×10^{17} Ti^+ cm^{-2} resulted in a mixture of final charge states, although in this case Ti^{4+} was the predominant state. However, given the surface specificity of the technique ($\sim$2 nm) it is possible that a large proportion of this state could have resulted either from surface structural relaxation or from reaction of the titanium at the surface with oxygen in the air. Attempts at removing this layer by argon ion sputtering only resulted in preferential removal of oxygen, thus altering the oxidation states present.

The channelled-RBS studies of Ti^+-implanted sapphire carried out by Farlow *et al.* [18] indicated that a sizeable proportion ($\sim$20%) of the titanium implanted occupied preferred substitutional sites within the sapphire structure. By comparison with similar studies carried out on Fe^+, Cu^+, Ni^+ and Cr^+ implanted sapphire these workers have inferred that a trivalent state is necessary for substitutionality. Thus, given the limitations of the EXAFS data and the uncertainty associated with the observations of Farlow *et al.* (i.e. are all the Ti^{3+} ions contained in substitutional sites?) there is broad agreement between the present work and the RBS studies.

From this background and the present study, it is now clear that some substantial fraction of the

titanium ions are present in the trivalent and divalent ionization states. Significant levels of Ti^{4+} states have not been observed though, based on the current models and observations (e.g. [6, 19]), this state should give the largest solid-solution hardening effect in sapphire. The observation [3] that both chromium and titanium ions implanted into sapphire also cause similar substantial hardening – and that chromium ions are expected to be present as predominantly Cr^{3+} [18] – thus suggest that radiation hardening is the dominant common mechanism with ion-specific solid-solution effects only making secondary contributions.

The observation that annealing significantly increases the proportion of Ti^{4+} could either reflect a change in the oxidation state of the implant species in the matrix or the incorporation of the titanium into the various precipitate phases reported to occur after this heat treatment [3]. Either possibility will require the absorption of charge-compensating oxygen from the atmosphere during the anneal. It is interesting that both the XANES and EXAFS data show the titanium to tend to a TiO_2 configuration since not only is TiO_2 the most thermodynamically stable of the titanium oxides at 1150° C [20] but it is also the precipitate phase expected at 1150° C from the equilibrium diagram [21], though the considerable disorder and damage in the system may cause departures from the equilibrium phases expected [3].

Any Ti^{4+} remaining in the α-Al_2O_3 matrix would be expected to give a significant solid-solution hardening effect though this would probably be masked by the hardening due to the precipitates.

In conclusion, we have been able to demonstrate that X-ray absorption techniques are a powerful means of providing charge state and site-environment information concerning the implanted species in ion-implanted ceramics even when the total implant concentration in the specimen volume is low. The information so gathered is, of necessity, averaged over the specimen volume but it is difficult to access this information in any other way. In the present case, XANES, EXAFS first shell radii and higher EXAFS shell information all suggest that the titanium ion implant exhibits varying (i.e. 2+ and 3+) charge states and is located in a variety of site types in a disordered Al_2O_3 matrix. After annealing at 1150° C, a trend towards the Ti^{4+} charge state in a more ordered environment was observed. Further detailed studies of both sapphire and other implanted ceramic systems, doses and damage states are being pursued and will form the basis of later reports.

Acknowledgements

We wish to thank SERC for provision of the SRS facility and for support. PJB and SJB wish to acknowledge SERC and AERE Harwell for the provision of CASE awards and AERE Harwell for later post-doctoral support (PJB). We also wish to thank Professors R.W.K. Honeycombe FRS, FEng, and D. Hull for provision of laboratory facilities, Dr. G. Dearnaley and Dr. N. Eyre for provision of technical assistance with the implantations and RBS analyses and GEC (Wembley, UK) for provision of the sapphire wafers. We are indebted to Dr. P. Hatton for his valuable assistance whilst at Daresbury.

References

1. G. DEARNALEY, *Thin Solid Films* **107** (1983) 315.
2. P. J. BURNETT and T. F. PAGE, *J. Mater. Sci.* **19** (1984) 3524.
3. *Idem*, in "Plastic Deformation of Ceramic Materials, II", edited by R. E. Tressler and R. C. Bradt (Plenum Press, New York, 1984) pp. 669–80.
4. C. J. MCHARGUE and C. S. YUST, *J. Amer. Ceram. Soc.* **67** (1984) 117.
5. P. J. BURNETT and T. F. PAGE, *J. Mater. Sci.* **19** (1984) 845.
6. T. E. MITCHELL and A. H. HEUER, *Mater. Sci. Eng.* **28** (1977) 81.
7. J. B. PENDRY, *Comm. Solid State Phys.* **X** (1983) 219.
8. P. A. LEE and J. B. PENDRY, *Phys. Rev.* **B11** (1975) 2795.
9. A. J. BOURDILLON, R. F. PETTIFER and E. A. MARSEGLIA, *J. Phys. C* **12** (1979) 3889–3897.
10. E. W. WHITE and H. A. MCKINSTRY, in "Advances in X-ray Analysis", edited by J. B. Newkirk and G. R. Mallett (Plenum Press, New York, 1966) p. 376.
11. B. K. TEO and P. A. LEE, *J. Amer. Chem. Soc.* **101** (1979) 2815.
12. A. J. BOURDILLON and G. P. TEBBY, *J. Microsc.* (1985).
13. G. P. TEBBY, A. J. BOURDILLON, R. T. PHILIPS and E. A. MARSEGLIA, in "EXAFS and Near Edge Structure III" edited by K. O. Hodgson, B. Hedman and J. G. Penner-Hahn, Springer Proc. Phys. Vol. 2 (Springer-Verlag, Berlin, 1984) pp. 86–8.
14. P. H. CITRIN, P. EISENBERGER and B. M. KINCAID, *Phys. Rev. Lett.* **36** (1976) 1346.
15. R. W. G. WYCKOFF, "Crystal Structures", 2nd Ed. (Wiley, New York, 1964).
16. A. PEREZ, M. TREILLEUX, P. THEVENARD, G. ABOUCHACRA, G. MAREST, L. FRITSCH and J. SERUGHETTI, *Proc. Mater. Res. Soc.* 7 (1982) 159.
17. P. J. BURNETT, PhD thesis, University of Cambridge (1984).
18. G. C. FARLOW, C. W. WHITE, C. J. MCHARGUE and B. R. APPLETON, *Proc. Mat. Res. Soc.* **27** (1984) 395.
19. B. J. PLETKA, T. E. MITCHELL and A. H. HEUER, in "Deformation of Ceramic Materials", edited R. C. Bradt and R. E. Tressler (Plenum Press, New York, 1975) pp. 181–94.
20. C. E. WICKS and F. E. BLOCK, in "US Bureau of Mines Bulletin 605" (US Government Printing Office Washington, 1963) p. 120.
21. E. M. LEVIN and H. E. MCMURDIE, in "Phase Diagrams for Ceramists, 1975 Supplement" (The American Ceramic Society, Columbus, Ohio, 1975) p. 135.

Received 20 May
and accepted 18 June 1985